International Journal of Engineering Trends and Technology
ISSN: 2231-5381/ https://doi.org/10.14445/22315381/IJETT-V74I10P107

Volume 74 Issue 10, 86-94, October 2026
© 2026 Seventh Sense Research Group®

Original Article

Corrosion Test Characterization of the Effects of Lamellar and Pitting Corrosion on Aluminum Alloys AA2024T3

Fatima Ezzohra EL GARCHANI[*1,2], Moulay Rachid KABIRI[1]

[1]*Engineering Sciences and Professions Laboratory, University Moulay Ismail, ENSAM, 50500, Meknes, Morocco,*
[2]*Research, Development and Innovation Laboratory, Mundiapolis University, Casablanca, Morocco.*

[*1]*Corresponding Author: f.ezzohra.elgarchani@gmail.com*

Received: 14 February 2026 Revised: 22 June 2026 Accepted: 22 July 2026 Published: 27 October 2026

Abstract *- The susceptibility of AA2024-T4 aluminum alloy to pitting and lamellar corrosion was investigated. The experimental study was conducted using EXCO immersion and anodic polarization tests at -720 mV in aerated and unventilated 1N H_2SO_4-based solutions, as well as salt spray tests at 20°C and 40°C. Forced convection using a drying oven at 80°C was carried out to assess weight loss. Electrical conductivity was measured using the eddy current method at frequencies of 60 kHz and 480 kHz. The results showed that the corrosion rate of the aluminum alloy increased with increasing temperature, whereas the forced convection drying oven test did not have a significant influence on the corrosion rate. Additionally, the evolution of electrical conductivity at depth, measured at 60 kHz, was generally positive, whereas a negative evolution was observed at the surface at 480 kHz. The effect of heat treatment on the microstructure of the AA2024-T3 alloy following the immersion test was also analyzed.*

Keywords *- Lamellar corrosion, Pitting corrosion, Forced convection drying oven, Electrical conductivity, Weight loss.*

1. Introduction

Despite the significant growth of composite materials, especially the Al-Cu-Mg alloy system, aluminum alloys are essential in the aircraft structures industry. This importance is essentially due to the exceptional balance they provide between mechanical characteristics on one hand and specific mass on the other. Indeed, one can reach the same levels of mechanical resistance with 1/3 of the mass for a structure made with this alloy as with steel [1, 2]. The mechanical properties of these alloys are primarily obtained through structural hardening treatments induced by thermo-mechanical processing that promotes precipitation hardening [3, 4].

In practice, each heat treatment corresponds to a specific metallurgical state with its own mechanical characteristics, including yield strength, fracture resistance, and fatigue strength [5]. At both manufacturing and maintenance stages, electrical conductivity and hardness are commonly used to characterize the metallurgical condition of the alloy [6]. The relationship between metallurgical state and electrical conductivity is well established, since conductivity strongly depends on the nature, spatial distribution, and volume fraction of the various intermetallic phases present in the matrix [7].

However, these strengthening precipitates generally possess corrosion potentials different from those of the aluminum matrix. Their presence therefore creates local electrochemical heterogeneities that promote selective localized corrosion, which is one of the most critical degradation mechanisms affecting these alloys [2, 8]. General corrosion is less frequent because of the spontaneous formation of a protective oxide film that slows down the corrosion process [9, 10]. Nevertheless, repeated breakdown and repassivation of this oxide layer may accelerate damage in aggressive environments. In real service conditions, such as marine atmospheres, airport coastal zones, humid industrial areas, and environments contaminated by chloride salts or de-icing agents, these localized corrosion phenomena become more severe and may significantly reduce structural durability.

The highly localized nature of corrosion attacks on aluminum aerospace alloys makes early detection particularly difficult for maintenance and structural health monitoring. The inaccessibility of affected zones, often located beneath coatings or external panels, combined with the small size of corrosion defects, considerably reduces the probability of detection using conventional non-destructive testing methods [11]. Consequently, there is a strong industrial need for

This is an open access article under the CC BY-NC-ND license (http://creativecommons.org/licenses/by-nc-nd/4.0/)

reliable indicators capable of identifying corrosion damage at an early stage before significant mechanical degradation occurs. In this context, monitoring approaches based on weight loss measurements and electrical conductivity obtained by eddy current testing offer a promising solution. These techniques provide valuable information on microstructural evolution, while corrosion-induced changes in precipitate distribution and matrix integrity may directly influence conductivity values. Moreover, eddy current inspection presents the practical advantage of being rapid, non-contact, and relatively insensitive to minor geometrical variations caused by section thinning.

Recent studies have confirmed that AA2024 alloy there are Cu-rich intermetallic particles and microgalvanic coupling effects in the structure, which makes remains highly susceptible to localized corrosion in chloride-containing environments [8]. Some investigators found that heat treatment strongly affects the distribution of precipitates, chemistry of grain boundaries, and hence the corrosion resistance [12].

Furthermore, more sophisticated methods like electrochemical impedance spectroscopy, polarization and eddy current inspection have been gaining research interest for early detection of corrosion in aerospace alloys [13]. There have been, however, few studies that have coupled the response of the electrical conductivity with the evolution of the mass loss with the morphology of the localized corrosion under combined accelerated environmental exposures typical of practical service conditions with heat treatment conditions. The corrosion behaviour of aluminum alloys has been subject of numerous studies, but little attention has been paid to the correlation of the morphological aspect of the localized corrosion with the development of the conductivity under accelerated conditions that are representative of real service conditions. The pitting corrosion and lamellar corrosion difference is not well studied for AA2024T3 alloy for combined exposure condition. This differentiation is of great practical relevance since pitting corrosion is typically seen as localized surface degradation while lamellar corrosion occurs under surface along microstructural interfaces, resulting in exfoliation, loss of cohesion, and massive weakening of the structure. The novelty of the present work is the use of immersion tests, the electrochemical techniques, salt spraying, forced convection drying cycles, and eddy current measurements to simulate realistic degradation environments and their effects on AA2024T3 alloy. Also, the study will correlate each corrosion mode to variations in mass loss, microstructural features and electrical conductivity response for useful indicators to early detection and condition monitoring. The present paper, therefore, focuses on the characterization of immersion corrosion, electrochemical testing, salt spray corrosion exposure test and forced convection drying oven cycles and aims to provide practical knowledge for maintenance strategies and the assessment of durability in the aerospace field.

2. Materials and Methods

2.1. Material

Aluminum alloy 2024-T3 (AA2024-T3) has been selected as the material test, its composition is given in Table1. Table 1. The chemical composition of the 2024-T351 aluminum alloy (wt%) is shown in the table. The table below shows the chemical composition of the 2024-T351 aluminum alloy (wt%).

Table 1. Chemical composition of AA2024-T3 aluminum alloy (wt%)

Element	Si	Fe	Cu	Mn	Mg	Cr	Zn	Ti	Al	Other
Composition%	0,5	0 ,5	3,8-4,9	0,3-0,9	1,2-1,8	0,1	0,25	0,15	90,7-94,7	0,05–0,15

2.2. Methods

2.2.1. EXCO Test

Test specimens were cut from AA2024T3 clad plates of both QQ-A-250/5 and QQ-A-250/13 types. The dimensions of the rectangular samples were 50 mm × 30 mm × 1.6 mm. Before testing, the surfaces were polished with a series of Silicon Carbide (SiC) abrasive papers from 400 to 1000 grit. In order to remove oxide layers and traces of corrosion that may have been present, the specimens were chemically cleaned by immersing them in a 10 wt.% NaOH solution (0.75 M) at 70°C for 30 s, followed by immersion in a 30 wt.% HNO_3 solution (68% purity) at 25°C for 30 s. Each specimen was then rinsed and dried, and its initial mass was measured. The exposure conditions consisted of two types of immersion tests. The first was carried out using the standardized EXCO test (ASTM G34), which is frequently used to assess the susceptibility of high-strength aluminum alloys to exfoliation corrosion.

The second test consisted of anodic polarization at −720 mV in 1N H_2SO_4 solutions under aerated and unventilated conditions. Aeration was provided by adding 30 mL H_2O_2 per liter of final solution. These procedures were selected to investigate the corrosion behavior of AA2024T3 under aggressive exposure conditions relevant to aerospace applications.

2.2.2. Electrical Conductivity Test

2 frequencies of 60 and 480 kHz were used to measure the electrical conductivity using the eddy current method, with the aim of investigating different penetration depths below the surface. Measurements were taken at the end of every exposure stage. Samples were first washed with demineralized water, dried and lightly ground to 600 grit to reduce the effect of corrosion roughening on the accuracy of the results. Three measurements were taken for each condition, and the average value reported.

2.2.3. Gravimetric Method

The difference between the sample's mass before and after corrosion testing was used to compute mass loss, which may be stated using the following formula:

$$\text{Mass loss} = \Delta m/m0 = (mf\text{-}mi)/mi$$

The samples were cleaned and dried in a dryer before to each measurement.

2.2.4. Accelerated Corrosion Tests

Three kinds of exposures were used for the accelerated corrosion tests:

Two salt spray tests in the cyclic corrosion test chamber marked Ascott following ASTM B 117-85, Neutral Salt Spray test (NSS) and the main parameters as shown in Table 2, at 20°C for a residence time of 64 hours and at 40°C for a residence time of 103.5 hours and a test in the forced convection drying oven, BINDER FD 115 at 80°C for 150 hours.

Table 2. Main parameters of neutral salt spray

Content of NaCl	50 g/l + 5g/l
Content of acetic acid	0
Content of CuCl2	0
pH	6-7.2

2.2.5. Heat Treatment

Table 3 gives details of the heat treatments carried out on AA2024 alloy, whose were immersed in a 3.5% saline solution as shown in Figure 1.

Table 3. Heat treatment conditions

Sample	**Treatments performed**
T0	Control sample
T1	Solution treatment at 495°C for 15 minutes and water quenching.
T2	Solution heated to 495°C for 15 minutes, quenched with water and tempered at 160°C

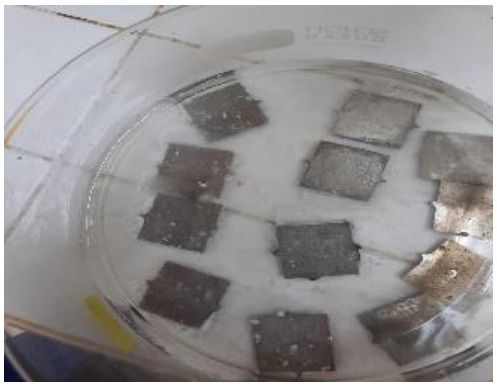

Fig. 1 AA2024 immersed in saline solution

2.2.6. Characterization

Optical Microscopy

Following the heat treatment and corrosion test, the microstructure was examined using an OLYMPUS BX60 optical microscope. Rectangular specimens with dimensions of 20 mm × 15 mm × 3 mm were used for metallographic observations. Keller's reagent, which is made up of 190 mL of distilled water, 2 mL of hydrofluoric acid, 3 mL of hydrochloric acid, and 5 mL of nitric acid, was used to etch the samples for 15 seconds. Prior to etching, the specimens were mechanically polished using emery sheets with sequential grit levels of 400, 600, 800, and 1200, followed by final polishing with a 6 µm diamond paste.

The Scanning Electron Microscope (SEM)

Surface morphology and intermetallic particle distribution were investigated using a JSM-IT500HR scanning electron microscope. Rectangular specimens with dimensions of 50 mm × 30 mm × 1.6 mm (surface area: 900 mm²) were analyzed before and after corrosion exposure. SEM observations were used to distinguish pitting corrosion from lamellar corrosion and to assess the severity of localized attack.

3. Results and Discussion

3.1. Microstructure of Aluminum Alloy 2024

Scanning electron microscopy observations in given in Figure 2. The S-Al2CuMg phase is represented by the first, which is spherical, while the second, which is somewhat darker in optical microscopy and has a more irregular form, is associated with larger particles.

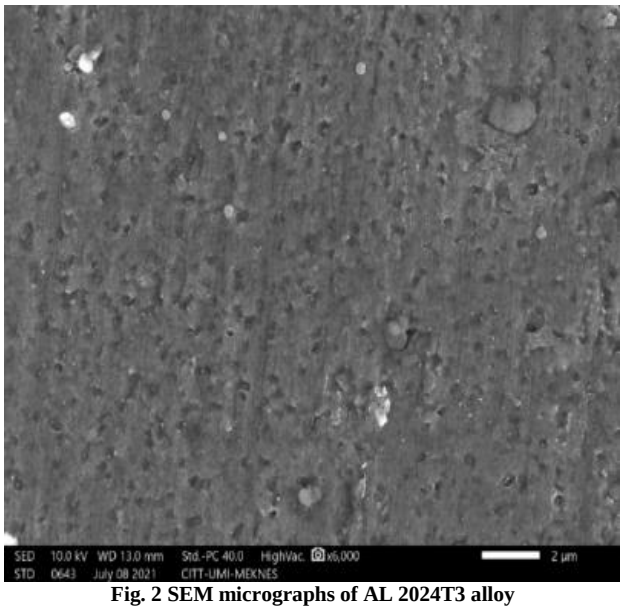

Fig. 2 SEM micrographs of AL 2024T3 alloy

These particles were identified as multiphase, Al-type particles (Cu, Mn, Fe, Si). These results are consistent with the literature [14-16].

3.2. Weight Loss of Al 2024-T3

Weight loss of Al2024-T3 as a function of exposure time in salt spray at 20°C, in salt spray at 40°C, and in the forced convection drying oven are shown in Figure 3.

In Figure 3(a), it can be seen that the result is that weight loss has increased. Based on the mass loss evolution as a function of exposure time, the corrosion behaviour of AA2024T3 alloy is strongly dependent on the temperature and the test environment. The first 20 h were also noted as a stabilization period at 20°C after which a slight mass loss of 0.00038% was observed after 28 h of exposure. After that, the weight loss gradually increased over time, reaching a maximum of 0.0024% for 57 h followed by a slight decrease. The trend implies that the native oxide film has a certain degree of protection at first, which is later reduced and then localized corrosion attack takes place. These same trends can be seen in Figures 3(b) and 3(c). Again, the first mass loss was observed at 40°C after 25 h, and this mass loss was 0.00038%. A temporary loss was then noticed, followed by stabilization from 43.5 h to 57.5 h, and then by a steady increase in mass loss. The higher temperature caused an increase in electrochemical reaction and the diffusion of chloride ions in the passive layer, which resulted in a higher corrosion rate when compared to the one obtained at 20°C. This validates the importance of temperature as a kinetic parameter in the degradation of AA2024T3 in a saline environment. For the oven test, the first measurable mass loss appeared after 46 h with a value of 0.0011%. The loss was then reduced to become insignificantly small between 70 h and 94 h of residence time, then increased steeply to a maximum of 0.048888% after 118 h of residence time and then slightly reduced. This action can be associated with cyclic processes of dehydration and cracking of the corrosion products, thus exposing fresh metallic surfaces to the oxidation process again. The oxide environment was not quite as corrosive as the salt spray environment, but thermal exposure can contribute to the microstructural instability and promote subsequent corrosion damage.

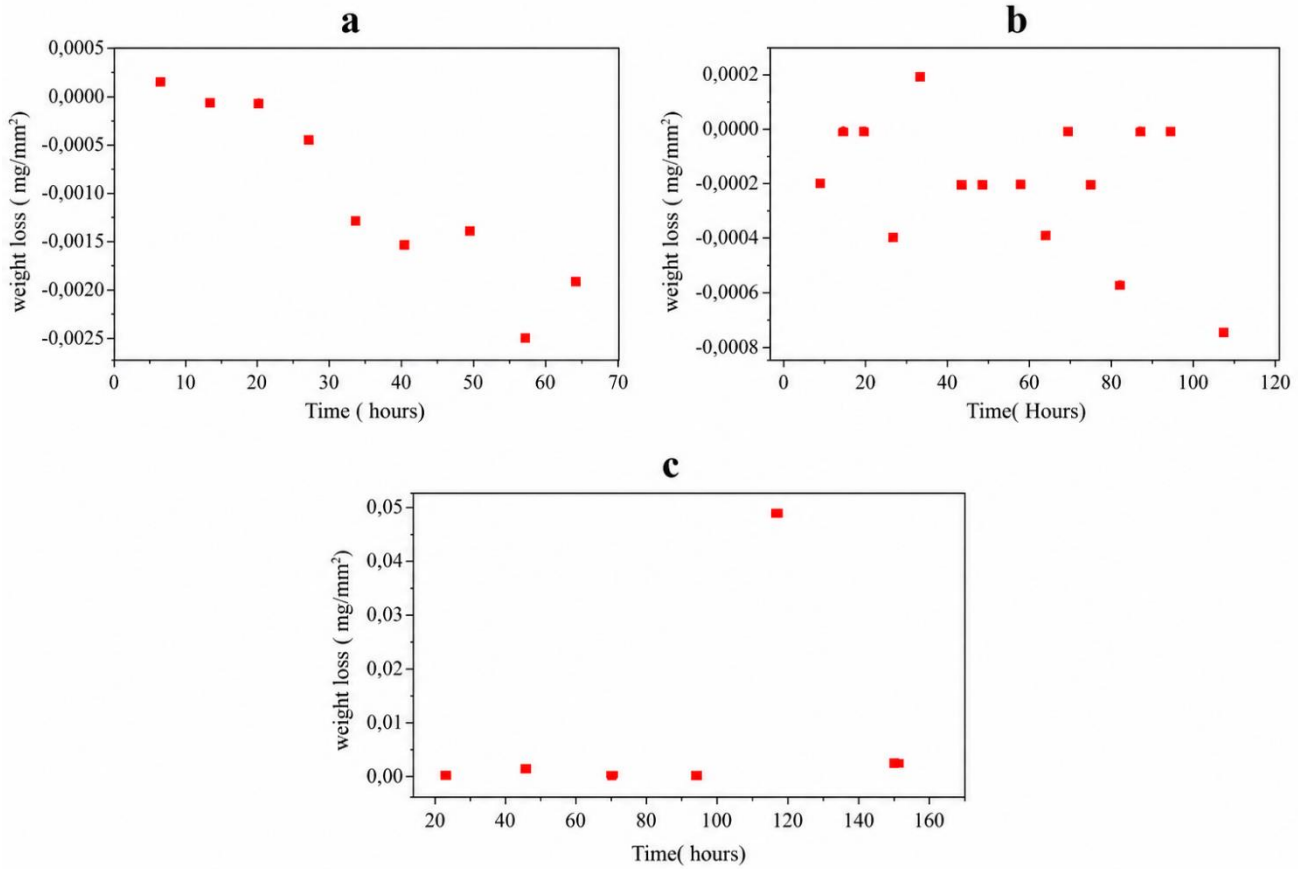

Fig. 3 Weight loss of AL2024T3 (a) Salt spray at 20°C, (b) Salt spray at 40°C, and (c) Forced convection drying oven.

The results obtained are in line with the observed behavior of aluminium alloys in chlorided environment. As the passive oxide film on aluminum is not thermodynamically stable in NaCl solutions, the presence of chloride ions allows penetration of the passive film and can cause localized breakdown. When the passive film is broken, aluminum dissolves as Al^{3+} ions, and the hydrolysis reactions in the occluded area acidify the pit and encourage pit growth [17].

This is because AA2024T3 contains a high level of copper and Cu-rich intermetallic particles that make it prone to pitting corrosion. These particles act as galvanic elements in the aluminum matrix and affect the initiation and propagation stages of pits. Coarse intermetallic particles ranging from 1 to 20 µm have been reported by several authors as being the preferential site for pitting nucleation due to interruption of continuity of the oxide film [18-22].

When looked at side by side, AA2024T3 is generally not as corrosion resistant as other alloys like AA6061 because it has a higher copper content, but it is less susceptible to stress corrosion cracking than other alloys like AA7075. But its great strength-to-weight ratio is also responsible for its ongoing presence in aerospace structures, where corrosion monitoring and preventive maintenance is still vital.

3.3. The Electrical Conductivity of Al 2024-T3

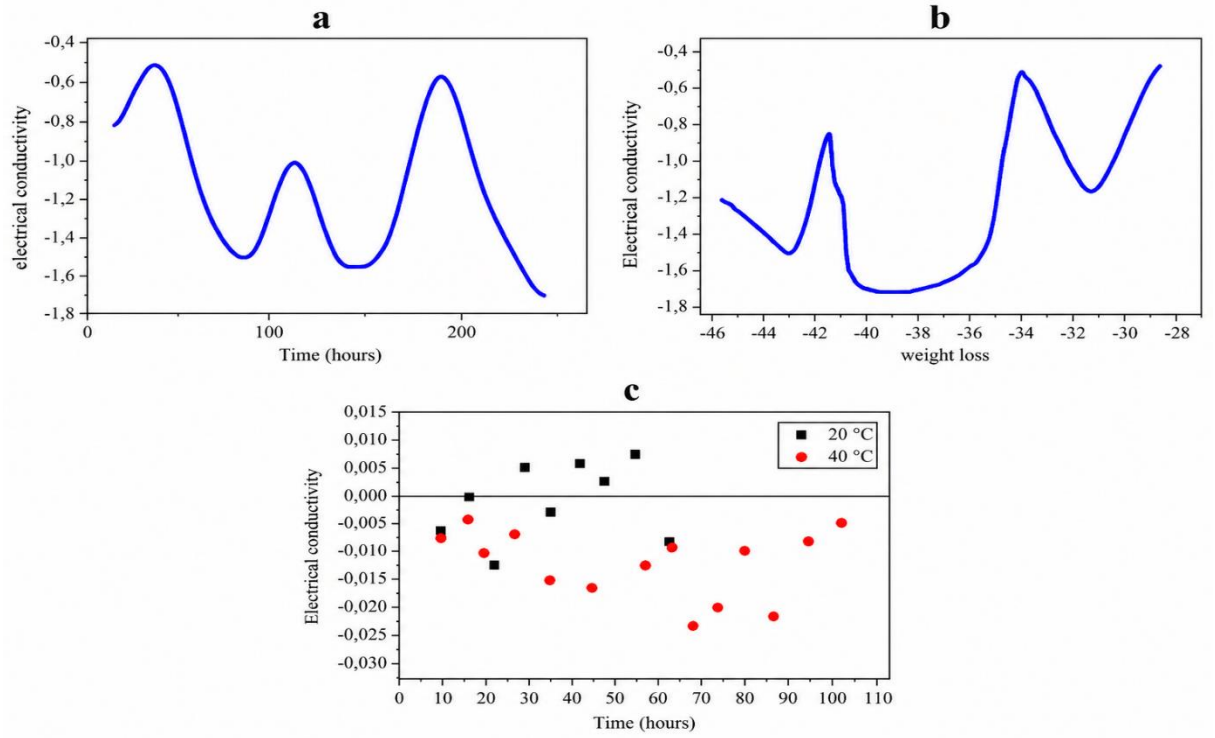

Fig. 4 (a) Variation of electrical conductivity for AL2024T3 in immersion, (b) Effect of mass on conductivity for 2024T3, and (c) Variation in electrical conductivity for 2024T3 in anodic polarization.

The evolution of the electrical conductivity as a function of time, observed on the 2024T3 alloy during the "EXCO test" immersion tests is measured by means of eddy currents, with a frequency of 60 KHz, are given in Figure 4. Time-varying patterns that alternate between regression and rise phases can be seen in Figure 4(a). The dissolution of magnesium, an element with a lower potential, initiates the dissolution of the secondary phases, which explains the oscillation between rising and declining electrical conductivity. This briefly increases the system's overall local electrical conductivity by enriching the zone with materials of higher conductivity (Cu). Following the completion of this sequence, the system's global conductivity experiences a period of regression as the remaining chemical element progressively dissipates in the solution.

This behavior is also visible in the effect of the evolution of the relative mass on the electrical conductivity of the material under study, as shown in Figure 4(b). In this figure, the conductivity of 2024T3 falls as a function of the decrease in the mass of the system. Contrary to the observations made for the immersion tests, the evolution of the electrical conductivity as a function of time during the electrochemical tests shows a concordance in the behavior of the alloy and the two frequencies, as shown in Figure 4(c).

The conductivity test results show similar variations (increase/decrease) as for the immersion test; therefore, the same explanation can be given for this behavior. Furthermore, the evolution in-depth (60 kHz) is globally positive, whereas it is negative at the surface (480 kHz). This difference explains the speed and capacity of penetration, which makes it likely that there is saturation, by sedimentation, of materials by chemical elements of high electrical conductivity at depth, as for the surface, the dissolution effect is complete, leading to a continuous drop in conductivity. The electrical conductivity evolution in the salt spray test of the AA2024 T3 alloy at 20°C is different from that at 40°C, as shown in Figure 5. In this

figure, the electrical conductivity shows both increases and decreases. The evolution at 20°C shows positive conductivities, while at 40°C; all conductivities have negative values, so this magnitude increases with decreasing temperature and decreases with increasing weight loss.

This difference is due to the speed of corrosion, which influences the electrical conductivity. For the forced convection drying oven test, the electrical conductivity does not behave the same way as in the previous tests.

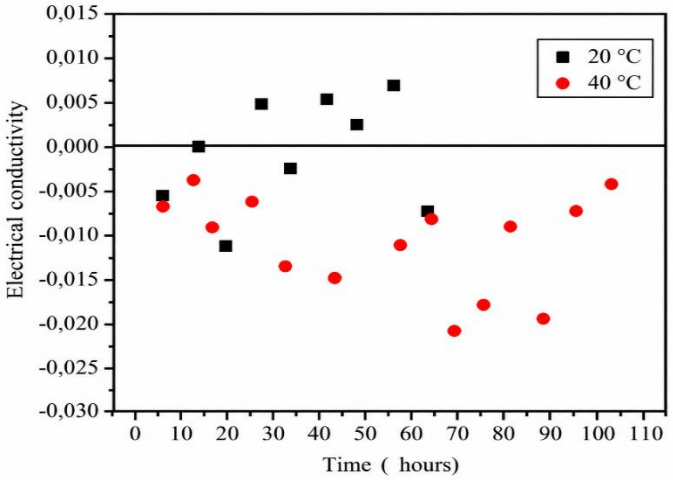

Fig. 5 Variation of the electrical conductivity of AA2024T3 in salt spray at 20°C and 40°C

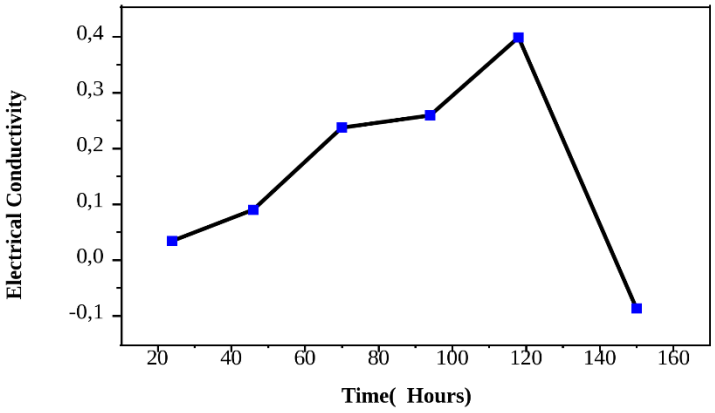

Fig. 6 Variation of the electrical conductivity of AA2024T3 in the forced convection drying oven

In Figure 6, we still have an increase in conductivity with time and increasing weight loss. The concordance between the material behaviors is due to the pitting corrosion induced by the electrochemical test, the accelerated corrosion tests (salt spray test and forced convection drying oven test) and lamellar corrosion induced by the EXCO test do not have the same effects insofar as pitting acts, for the most part, on the secondary phases located inside the grains while exfoliation acts on the precipitates present within the grain joints.

3.4. Effect of Heat Treatment on Mass Loss in AA2024 T3 Alloy after Immersion Test

The mass loss for each heat treatment was measured. Immersion of the samples was done in a 5% NaCl saline solution. Figure 7 illustrates how the mass loss changes for the different heat treatments in relation to immersion time.

In contrast to the other curves, curve T2 represents the artificial aging therapy curve. Compared to the other treatments, where the solid-liquid interface deteriorated due to alloy oxidation, its mass loss is significantly greater. The artificially aged sample thus exhibits greater corrosion resistance than the T0 and T1 samples. In aging test, Meyveci et al. [23-26] found that the wear resistance of AA 2024 aluminum alloys decreased. The samples with the most mass loss were those aged at 220°C. However, samples of AA 2024 aluminum alloy that had been aged at 180°C and had the highest hardness values demonstrated the best resistance to wear. The mass loss decreases with age. This is the normal course of aging. Figure 8 shows a T2 sample extracted after 1200 hours of immersion, clearly showing the presence of pitting due to deterioration of the AL2O3 passive film after Cl attack.

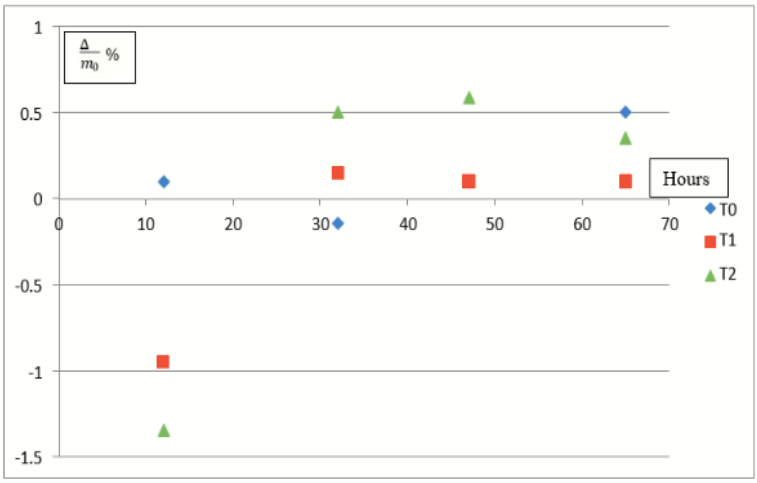

Fig. 7 Sample mass variation during immersion tests

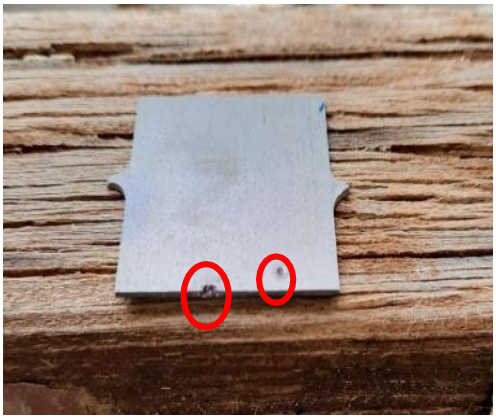

Fig. 8 Bare-eye observation of a T2 sample after 1200 hours of immersion

3.5. Effect of Heat Treatment on the Microstructure of AA2024 T3 Alloy after Immersion Test

The surface morphology of different heat treatment conditions of the AA2024 alloy after immersion test was analyzed, as shown in Figure 9. All specimens had localized pitting corrosion, with varying intensity and density of pits related to the heat treatment condition and immersion time. The intensity of pitting decreased with increased immersion times. The immersion test enabled the simulation of the possible effects of marine service environments on the AA2024 alloy, especially in chloride-rich environments. The alloy was highly susceptible to localized corrosion, whether the heat treatment applied was T5 or T83.After exposure to the corrosive medium, the alloy had a high tendency to localized corrosion, with pit initiation occurring within the first days of exposure, irrespective of the heat treatment applied (T5 or T83). This confirms the sensitivity of AA2024 to chloride attack, mainly due to the presence of Cu-rich intermetallic particles that promote galvanic interactions with the aluminum matrix. The decrease of pits seen after long immersion time may be attributed to one or more of the following mechanisms. First, the pitting corrosion is localized and non-uniformly distributed over the specimen surface. This means that the area being examined may not necessarily be the area with the worst attacks. Secondly, corrosion products and salt deposits could be deposited on the surface, partially covering existing pits and altering the apparent density of the pits.

Under-deposit corrosion can also occur with such deposits, allowing local corrosion to persist under the accumulation of salts, but not be as obvious at the surface. Microstructural modifications are also another effect that heat treatment has on corrosion morphology. The size, distribution, and composition of the precipitates and the grain boundary chemistry can be altered by solution treatment and aging conditions, which will influence the susceptibility to pit nucleation. Data obtained from comparative observations indicate that the treated samples with a more uniform distribution of precipitates had lower pit density than the untreated condition. In practical terms, these findings suggest that AA2024 continues to be susceptible, even after optimization of heat treatment, when exposed to marine and/or humid chloride-containing environments. Therefore, early detection of corrosion, regular checking and protective coatings are necessary to guarantee the durability of the structures in aerospace and coastal applications.

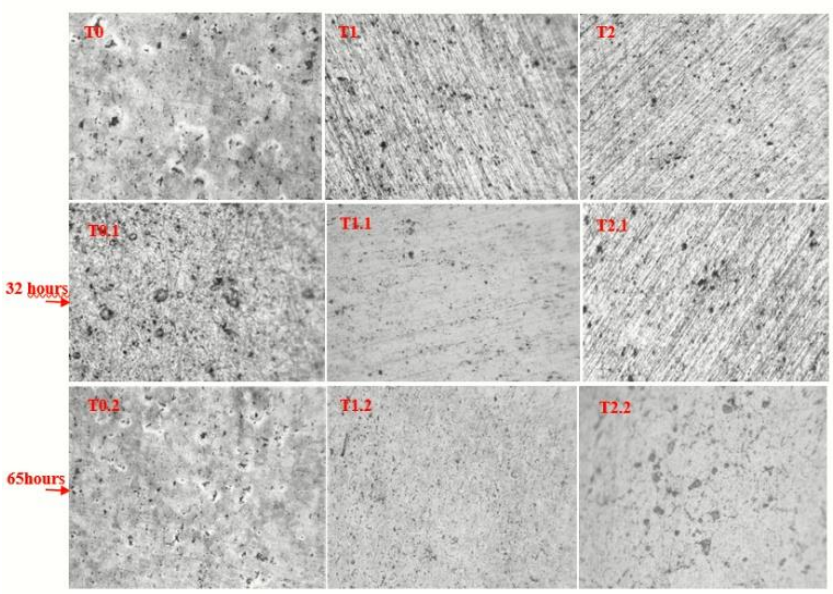

Fig. 9 Micrographs of the various samples studied during the tests, as a function of immersion period

4. Conclusion

In the present study, it was possible to establish, by monitoring the evolution of weight loss and electrical conductivity of 2024T3 aluminum alloys, that they do not show the same behavior during exfoliation.

This observation is confirmed by the results obtained by comparing this evolution with the variation of the relative mass and electrical conductivity of 2024T3, which decreases with the regression of the relative mass. This difference in behavior did not occur in the case of pitting corrosion. However, in this case of electrical conductivity, it shows a negative evolution at the surface level on the spot when this evolution is positive in depth.

Conflicts of Interest

The authors declare that there is no conflict of interest regarding the publication of this paper.

References

[1] Robert L. Ferry, and J. Randolph Kissell, *Aluminum Structures: A Guide to Their Specifications and Design*, John Wiley et Sons Ltd, 2022. [Google Scholar] [Publisher Link]

[2] Christian Vargel, *Corrosion of Aluminium*, 2nd Ed., Elsevier, 2022. [CrossRef] [Google Scholar] [Publisher Link]

[3] Vakpak65 Containers and Wraps, VakCo Heat Treating Supplies, 2022. [Online]. Available: https://vakcousa.com/vakpak65-containers-and-wraps/

[4] H. Sehitoglu, T. Foglesong, and H.J. Maier, "Precipitate Effects on the Mechanical Behavior of Aluminum Copper Alloys: Part I. Experiments," *Metallurgical and Materials Transactions A*, vol. 36, no. 3, pp. 749-761, 2005. [CrossRef] [Google Scholar] [Publisher Link]

[5] AMS2770 Heat Treatment of Aluminum and Aluminum-base Alloys, 2022. [Online]. Available : https://saemobilus.sae.org/standards/ams2770-heat-treatment-aluminum-aluminum-base-alloys

[6] Benedetta M. Kikechi, "*Evaluation of Effectiveness of Non Destructive Testing Techniques for Inspection of Critical Aircraft Components-A Case of the Kenyan Aviation Industry*," University of Nairobi, pp. 1-117, 2020. [Publisher Link]

[7] J.Y. Barghout et al., "The Effects of Second Phase Particles, Dislocation Density and Grain Boundaries on the Electrical Conductivity of Aluminium Alloys," *Materials Science Forum*, vol. 217-222, pp. 975-980, 1996. [CrossRef] [Google Scholar] [Publisher Link]

[8] N. Birbilis and R.G. Buchheit, "Electrochemical Characteristics of Intermetallic Phases in Aluminum Alloys: An Experimental Survey and Discussion," *Journal of the Electrochemical Society*, vol. 152, no. 4, pp. 1-12, 2025. [CrossRef] [Google Scholar] [Publisher Link]

[9] J. Soltis, "Passivity Breakdown, Pit Initiation and Propagation of Pits in Metallic Materials – Review," *Corrosion Science*, vol. 90, pp. 5-22, 2015. [CrossRef] [Google Scholar] [Publisher Link]

[10] L.C. Abodi et al., "Modeling Localized Aluminum Alloy Corrosion in Chloride Solutions Under Non-Equilibrium Conditions: Steps Toward Understanding Pitting Initiation," *Electrochimica Acta*, vol. 63, pp. 169-178, 2012. [CrossRef] [Google Scholar] [Publisher Link]

[11] R.T.O. AGARDograph, "*Corrosion Fatigue and Environmentally Assisted Cracking in Aging Military Vehicles*, Technical Report AG–AVT–140, NATO, 2011. [Google Scholar] [Publisher Link]

[12] J.R. Davis, *Corrosion of Aluminum and Aluminum Alloys*, ASM Technical Books, 1999. [CrossRef] [Google Scholar] [Publisher Link]
[13] Christophe Laurent et al., "The Contribution of Hydrogen Evolution Processes during Corrosion of Aluminium and Aluminium Alloys Investigated by Potentiodynamic Polarisation Coupled with Real-Time Hydrogen Measurement," *Npj Materials Degradation*, vol. 1, no. 1, pp. 1-7, 2017. [CrossRef] [Google Scholar] [Publisher Link]
[14] Chi-Min Liao, and Robert P. Wei, "Galvanic Coupling of Model Alloys to Aluminum — A Foundation for Understanding Particle-Induced Pitting in Aluminum Alloys," *Electrochimica Acta*, vol. 45, no. 6, pp. 881-888, 1999. [CrossRef] [Google Scholar] [Publisher Link]
[15] R.G. Buchheit et al., "Local Dissolution Phenomena Associated with S Phase (Al_2CuMg) Particles in Aluminum Alloy 2024-T3," *Journal of The Electrochemical Society*, vol. 144, no. 8, pp. 2621-2628, 1997. [CrossRef] [Google Scholar] [Publisher Link]
[16] Valérie Guillaumin, and Georges Mankowski, "Localized Corrosion of 6056 T6 Aluminium Alloy in Chloride Media," *Corrosion Science*, vol. 42, no. 1, pp. 105-125, 2000. [CrossRef] [Google Scholar] [Publisher Link]
[17] M. Reboul and J. Bouvaist, "Study of the Mechanism of Layering Corrosion of Aluminum Alloy 7020," *Pascal and Francis Bibliographic Databases*, 1980. [Google Scholar] [Publisher Link]
[18] George E. Thompson, "Corrosion and Filming Behaviour of Aluminium and its Alloys," *Materials Science Forum*, vol. 217-222, pp. 95-106, 1996. [CrossRef] [Google Scholar] [Publisher Link]
[19] Robert P. Wei, Chi-Min Liao, and Ming Gao, "A Transmission Electron Microscopy Study of Constituent-Particle-Induced Corrosion in 7075-T6 and 2024-T3 Aluminum Alloys," *Metallurgical and Materials Transactions A*, vol. 29, no. 4, pp. 1153-1160, 1998. [CrossRef] [Google Scholar] [Publisher Link]
[20] Joffrey Tardelli, "*Study of the Electrochemical Behavior of the Intermetallic Phases of 2214-T6 and 7050-T74 Aluminum Alloys: A Multi-Scale Approach to Polyphase Materials*," Doctoral thesis, University of Lorraine, 2012. [CrossRef] [Google Scholar] [Publisher Link]
[21] A. Boag et al., "Corrosion of AA2024-T3 Part I: Localised Corrosion of Isolated IM Particles," *Corrosion Science*, vol. 53, no. 1, pp. 17-26, 2011. [CrossRef] [Google Scholar] [Publisher Link]
[22] Minhua Shao et al., "A Study on Pitting Corrosion of Aluminum Alloy 2024-T3 by Scanning Microreference Electrode Technique," *Materials Science and Engineering: A*, vol. 344, no. 1-2, pp. 323-327, 2003. [CrossRef] [Google Scholar] [Publisher Link]
[23] Thang Le Toan, and Nguyen Van Cuong, "Evaluation of the Mechanical Properties and the Corrosion Resistance of the Cobalt-Base Alloy Stellite 6 on 1045 Steel by Laser Cladding," *Engineering, Technology and Applied Science Research*, vol. 15, no. 3, pp. 23323-23329, 2025. [CrossRef] [Google Scholar] [Publisher Link]
[24] Teguh Dwi Widodo et al., "The Effect of Coating Procedure on the Strength and Corrosion Resistance of Epoxy Coatings on A36 Steel: Pull-Out and Potentiodynamic Analysis," *Engineering, Technology and Applied Science Research*, vol. 15, no. 5, pp. 27096-27104, 2025. [CrossRef] [Google Scholar] [Publisher Link]
[25] I. Alenezi, "Effects of Heat Treatment on the Corrosion Behavior of ASTM A-36 Steel," *Engineering, Technology and Applied Science Research*, vol. 10, no. 1, pp. 5320-5324, 2025. [CrossRef] [Google Scholar] [Publisher Link]
[26] Asma Mahdi Ali, Luma Fadhil Hussein, and Raghad Mohammed Khudada, "The Behavior of Corroded Reinforced Concrete Beams under External Loads: A Literature Review," *Engineering, Technology and Applied Science Research*, vol. 15, no. 5, pp. 27872-27876, 2025. [CrossRef] [Google Scholar] [Publisher Link]